Journal of Power Sources 266 (2014) 60–65

Contents lists available at ScienceDirect

Journal of Power Sources

journal homepage: www.elsevier.com/locate/jpowsour

Short communication

Enhancing the high-rate performance of $Li_4Ti_5O_{12}$ anode material for lithium-ion battery by a wet ball milling assisted solid-state reaction and ultra-high speed nano-pulverization

Zhao Huang [a], Dan Wang [b], Ye Lin [c], Xiaoyan Wu [b], Peng Yan [b], Chunming Zhang [b,*], Dannong He [a,b,*]

[a] School of Material Science and Engineering, Shanghai Jiaotong University, No.800 Dongchuan Road, Shanghai 200240, PR China
[b] National Engineering Research Center for Nanotechnology, No.28 East Jiangchuan Road, Shanghai, 200241, PR China
[c] Solid Oxide Fuel Cell SmartState Center, University of South Carolina, 541 Main Street, Columbia, SC 29208, USA

HIGHLIGHTS

- A modified solid-state reaction method with in situ coating process is investigated.
- The ultra-high speed nano-pulverization pretreatment process was introduced.
- The obtained $Li_4Ti_5O_{12}$ electrode material showed high surface area and dispersion.
- The treated $Li_4Ti_5O_{12}$ showed excellent electrochemical performance.

ARTICLE INFO

Article history:
Received 26 January 2014
Received in revised form
11 April 2014
Accepted 30 April 2014
Available online 14 May 2014

Keywords:
Lithium titanate
Anode material
Li-ion battery
Ultra-high speed nano-pulverization

ABSTRACT

$Li_4Ti_5O_{12}$ was successfully synthesized by a modified solid-state reaction method with an in situ coating process. The powders were characterized by X-ray diffraction, BET surface area and scanning electron microscopy. Sub-micron $Li_4Ti_5O_{12}$ oxides, with a high phase purity and accurate stoichiometry, were obtained after calcination at 800 °C for 7 h. The pure $Li_4Ti_5O_{12}$ electrode material showed a much higher surface area and specific capacity than the one without the ultra-high speed nano-pulverization pretreatment process. Excellent reversible high-rate capability was achieved as 137 mAh g^{-1} at 10C, 107 mAh g^{-1} at 20C, 76 mAh g^{-1} at 40C. The result of the cycling performance showed high capacity retention of about 100% for all charge/discharge rates after 10 cycles. Electrochemical impedance spectra tests demonstrated that the lithium-ion diffusivity in $Li_4Ti_5O_{12}$ was improved significantly after the pretreatment, which indicated that the ultra-high speed nano-pulverization treated $Li_4Ti_5O_{12}$ with high dispersion and smooth particle surface would be a promising high-rate anode material for lithium-ion battery.

1. Introduction

Nowadays, the spinel $Li_4Ti_5O_{12}$ has been considered as an alternative candidate for the anode material of solid, liquid and gel Li-ion batteries because of its unique characteristics, such as good structural stability with nearly zero strain upon the intercalation/deintercalation of Li^+, a flat operating potential at about 1.55 V vs. Li^+/Li and an excellent cycling performance [1–6]. Despite these advantages mentioned above, however, the low electrical conductivity (10^{-9} S cm^{-1}) and Li-ion diffusion coefficient of $Li_4Ti_5O_{12}$ results in poor rate capability [7,8]. Many approaches have been developed to overcome these shortcomings and then improve the battery performance, including reducing the particle size [9–11], improving the electrical conductivity by surface modification [4,12–16] and ion doping [17–21]. Among these methods, reducing the particle size is one of the most effective ways to increase the contact area between electrode and electrolyte, and also to shorten the diffusion length of lithium-ions and electrons.

$Li_4Ti_5O_{12}$ powders are mainly prepared by a conventional solid-state reaction (SSR) of lithium and titanium salts followed by higher calcination processes between 800 and 1100 °C [22–26], which

* Corresponding authors. National Engineering Research Center for Nanotechnology, No.28 East Jiangchuan Road, Shanghai, 200241, PR China. Tel.: +86 21 34291286; fax: +86 21 34291125.
E-mail addresses: zhangchm2003@163.com (C. Zhang), hdnbill@sh163.net (D. He).

http://dx.doi.org/10.1016/j.jpowsour.2014.04.146
0378-7753/

would introduce several disadvantages, including low homogeneity, irregular morphology, large particle size and long calcination time. Besides, it is difficult to reduce the particle size using the SSR method. In order to significantly intensify the dispersion and surface area of $Li_4Ti_5O_{12}$ and further enhance its conductivity, two methods are proposed: (1) improving the synthesis route to get nano-particles, including adding some dispersing agents or nano-filler to prevent the nanoparticles aggregating or growth [27,28]; (2) applying the mechanical force in ultra-fine grinding to induce the chemical/physical reaction [1,29]. In these ways, the particle size of $Li_4Ti_5O_{12}$ material is finally reduced, and then the improved performance of the electrode at a high charge/discharge rate is achieved.

In this paper, we report the synthesis of sub-micron sized material via a facile in situ $TiO_2 \cdot H_2O$ coating process by applying the mechanical force in ultra-high speed nano-pulverization assisted SSR method (USN-SSR). The precursors were then sintered at various temperatures. The prepared samples using SSR and USN-SSR method were simultaneously characterized by X-ray diffraction (XRD), BET and scanning electron microscopy (SEM) in order to examine the phase structure, the specific surface area and morphology differences, respectively. The electrochemical performance of the prepared $Li_4Ti_5O_{12}$ electrode materials was also investigated by a half-cell system.

2. Experimental

$Li_4Ti_5O_{12}$ was successfully synthesized from Li_2CO_3 and tetrabutyl titanate by a modified solid-state method. Appropriate amounts of OP9, HNO_3, Li_2CO_3 and ethanol were thoroughly mixed, and then tetrabutyl titanate [$Ti(C_4H_9O)_4$, TBT] (the mole ratio of Li to Ti is 4.04:5) was slowly introduced using a dropper with the speed of 5 mL min^{-1}. OP9 was first dispersed into ethanol to form micelles. Then stir in Li_2CO_3 and TBT until evenly dispersed. To reduce the speed of the TBT hydrolysis, HNO_3 was added to this solution prior to TBT's admission. And then the obtained solution was dispersed in agate jar and well mixed by ball milling using agate balls. The milling was performed in air at 400 rpm rotational speed for 10 h. The precursor of $TiO_2 \cdot xH_2O$ (the hydrolysis product of TBT) coated Li_2CO_3 was heated at 80 °C for 12 h in a drying oven. Finally, it was sintered at 800 °C for 7 h in air and then smashed at Mach 1.5 for 1 h by USN processing equipment (LXZ Spraying & Purification Technology Co., Ltd, China) to prepare the porous $Li_4Ti_5O_{12}$. Due to the effect of centrifugal force, material slams the outer limits of crushing cavity for secondary collisions, and then falls into the pulverizer to continue multiple shear. It is worth noting that USN process can greatly decrease the particle size while the material's Mohs hardness is less than 4.0. If the material's Mohs hardness is greater than 4.0, the effect of USN process on the particle size is not obvious. However, it will influence the materials microtopography, such as the good particle smoothness, regulation, activation and dispers. The straightforward synthesis strategy for $Li_4Ti_5O_{12}$ is schematically depicted in Fig. 1.

The electrochemical cells consisted of Li metal as the anode, $Li_4Ti_5O_{12}$ based composite as the cathode and 1 M solution of $LiPF_6$ dissolved in a 1:1 mixture by volume of ethylene carbonate (EC) and dimethyl carbonate (DMC) as the electrolyte. Microporous polypropylene sheet (Celgard, 2400) was used as the separator. The working electrode was fabricated by mixing 85:10:5 (w/w) ratio of $Li_4Ti_5O_{12}$ active material, a carbon (acetylene black) electronic conductor and polyvinylidene fluoride (PVDF) binder in N-methyl-2-pyrrolidinone (NMP). The slurry was then coated on the copper foil (~10 μm) current collector and dried under vacuum at 120 °C for 12 h. The next step was to compress the electrode plate and then cut it to many small plates of 11 mm diameter (the active material is about 1.7 mg). The cells were assembled in pure argon protected glove box in which water content was kept below 0.1 ppm.

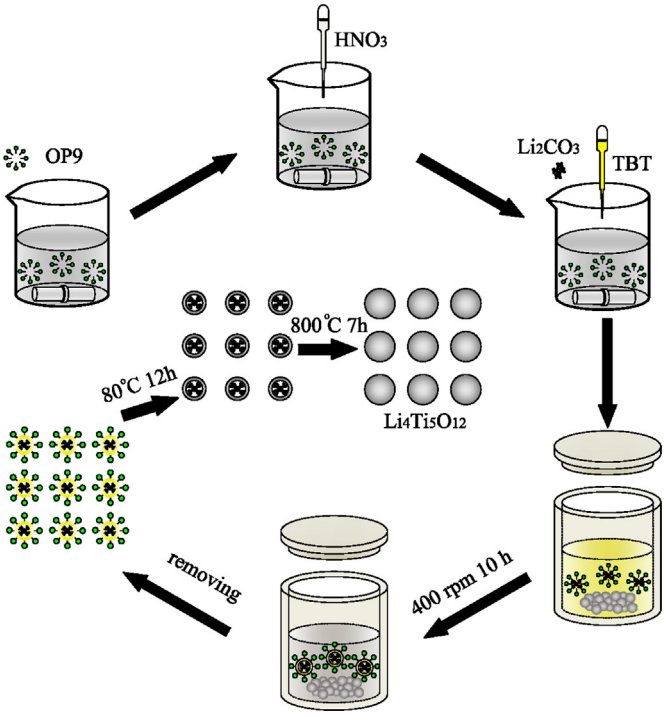

Fig. 1. Schematic illustration of the formation of $Li_4Ti_5O_{12}$ through a modified solid-state reaction method with in situ coating process approach.

The crystal structures of the fresh $Li_4Ti_5O_{12}$ powders were examined by XRD using a Bruker D8 advance diffractometer with nickel filtered Cu kα radiation ($\lambda = 1.5418$ Å) over the 2θ range from 10° to 80°. The particle morphology was observed using JEOL-6930 scanning electron microscopy (SEM). The specific surface area of the samples was determined by N_2 adsorption using a 3H-2000 specific surface area instrument (Beishide Instrument-ST Co., Ltd., Beijing, China). The samples were treated at 200 °C for 3–5 h in a vacuum to remove the surface adsorbed species. The charge/discharge performance of the cells were performed over the potential range between 1.0 and 3.0 V using a NEWARE BTS 5 V-10 mA computer-controlled Galvanostat (Shenzhen, China) at different rates of 0.5–40C at room temperature. Electrochemical impedance spectroscopy (EIS) was carried out using CHI660B electrochemical workstation (Shanghai Chenhua Instrument Co. Ltd., China) in the frequency range from 0.1 Hz to 1 MHz. All the cells were first shelving at open circuit voltage state for 10 h at 25 °C.

3. Results and discussion

3.1. Powder characterization

To verify whether the in situ coating process of amorphous $TiO_2 \cdot xH_2O$ coated onto Li_2CO_3 can prevent intergranular reunion among the $Li_4Ti_5O_{12}$ particles, TEM was carried out on morphology of the precursor powders. It is well known that the product of TBT hydrolysis is $TiO_2 \cdot xH_2O$. As shown in Fig. 2, the $TiO_2 \cdot xH_2O$ sample exhibits a uniform fine-colloidal microstructure, which is conducive to the synthesis of $Li_4Ti_5O_{12}$ fine powders. Fig. 2 also shows the spherical $LiCO_3$ powders are well dispersed into the body of amorphous $TiO_2 \cdot xH_2O$. Furthermore, $TiO_2 \cdot xH_2O$ coating may help inhibit the $Li_4Ti_5O_{12}$ grain growing up during sintering.

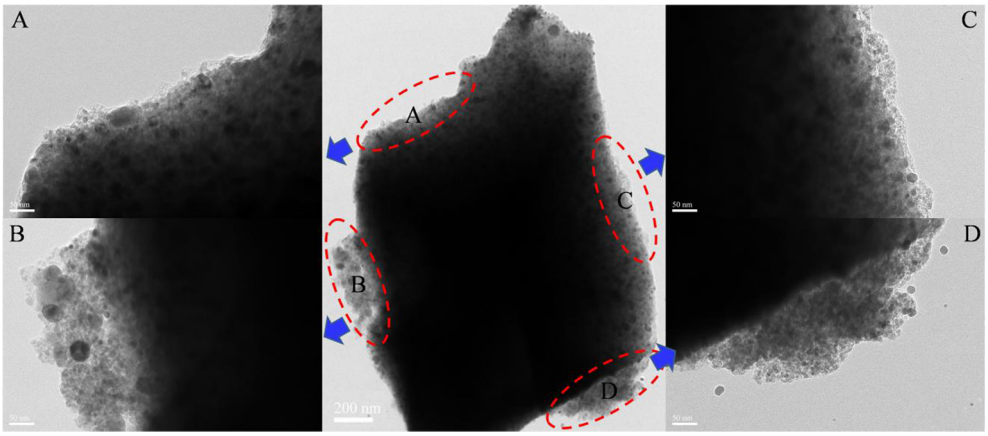

Fig. 2. TEM images of the obtained the precursor of $TiO_2 \cdot xH_2O$ coated Li_2CO_3.

Then the X-ray diffraction pattern of the synthesized $Li_4Ti_5O_{12}$ samples with in situ coating process fired at different temperatures are shown in Fig. 3. The precursor of $TiO_2 \cdot xH_2O$ coated Li_2CO_3 shows an amorphous structure. At 500 °C, the diffraction peaks corresponding to the intermediate phase anatase TiO_2, some impurity substances and spinel $Li_4Ti_5O_{12}$ phase begin to appear. It also shows the intensity of the diffraction peaks of $Li_4Ti_5O_{12}$ phase is gradually enhanced and rutile TiO_2 phase sharply decreased with increasing the firing temperature more than 500 °C, which further indicates the crystallinity and grain size of $Li_4Ti_5O_{12}$ are increasing with the increasing of the calcination temperatures. Fig. 3 also shows the XRD patterns of the samples before and after USN treatment. The diffraction peaks of two investigated samples can be indexed in the Fd-3m space group with a cubic spinel structure and no impurity peaks, indicating that the USN treatment did not change the sample's structural characteristics. However, the XRD peak intensities decrease after the USN treatment, indicating the relatively poor crystallinity of $Li_4Ti_5O_{12}$ after USN treatment. This is because the adjacent atoms bond ruptured and the strong atomic bonding force released under mechanical loading. It is easy to be activated in spontaneously formed new surface. Thus, the increase

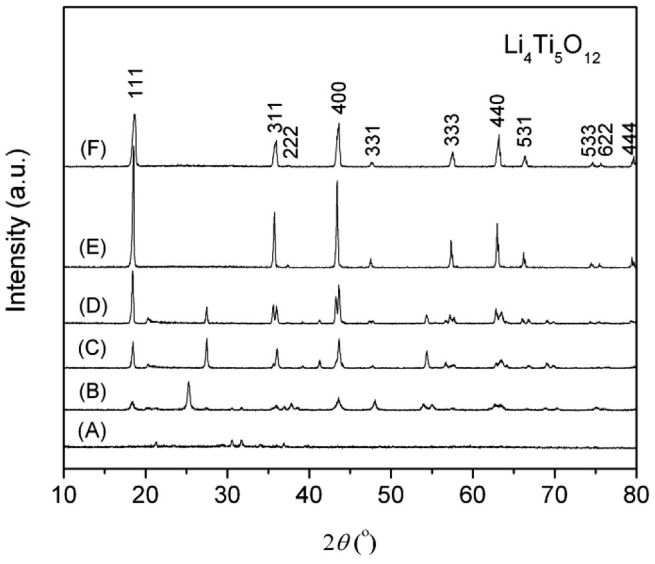

Fig. 3. The X-ray diffraction pattern of $Li_4Ti_5O_{12}$ samples calcined at different temperatures for 7 h (A) precursor dried at 120 °C, (B) 500 °C, (C) 600 °C, (D) 700 °C, (E) 800 °C, (F) after the USN processing.

of surface energy and mechanical activation could result in the spontaneous restructuring of the particle surface structure, and then lead to the formation of some amorphous structure. The dimensions of sub-micron $Li_4Ti_5O_{12}$ are estimated using the Scherrer formula based on the widths of the major diffraction peaks observed in Fig. 3 while the firing temperature is 800 °C for 7 h. Calculated from the full width at half maximum (FWHM) of the XRD reflection peaks, the grain size of $Li_4Ti_5O_{12}$ are 67 nm (111), 84 nm (311), 107 nm (400), 96 nm (440), respectively. Furthermore, the pure phase $Li_4Ti_5O_{12}$ can be obtained by using less lithium source, while the initial mole ratio of Li to Ti is 4.04:5, which is less than the other reported results [21,30].

Although, theoretically, in situ coating process and the results of calculation based on Fig. 3 would produce smaller grain size of $Li_4Ti_5O_{12}$ powder, however, there are still some drawbacks of this method. Some $Li_4Ti_5O_{12}$ particles in Fig. 4A and B have formed large agglomerations due to the high calcination temperature. On the other hand, Fig. 4C and D shows that $Li_4Ti_5O_{12}$ powders after the USN retreating have high dispersion and roundish spherical structure. Compared with the above sample the particles have relatively much less agglomerations. This feature by shearing and tearing the pristine powders were using the boron carbide grinding tool with very high speed in grinding chamber during the process. In Fig. 4, both the size of primary particles with and without the USN processing is fairly small, and the USN processing did not result in significant change of the particles size. But, powders derived from this method have very smooth surface and high surface area. The specific surface area of $Li_4Ti_5O_{12}$ samples with and without the pretreatment are 3.4 $m^2\ g^{-1}$ and 1.5 $m^2\ g^{-1}$, respectively. As we know, the particle size of commercial electrode materials is mostly controlled in the sub-micron range. Therefore, in order to keep the particle size of $Li_4Ti_5O_{12}$ in the original sub-micron range, the treating time is strictly controlled.

Then, dispersion situation of particle was studied by comparing the status of the powder deposition in suspension after the ultrasonic. Fig. 5A and B images show freshly prepared $Li_4Ti_5O_{12}$ powder's colloidal suspensions and suspensions aged at room temperature for 5 days, respectively. "a" represents the powder slurry treated with USN, "b" represents the powder slurry without USN processing. After the ageing, the $Li_4Ti_5O_{12}$ powders with USN processing did not display obviously sedimentation, while the original $Li_4Ti_5O_{12}$ powders separated from deionized water. The high stability of the treated $Li_4Ti_5O_{12}$ powders colloidal suspension was attributed to its fine particle sizes and high dispersion, which contended with sedimentation by Brownian motion. Because of the high degree of $Li_4Ti_5O_{12}$ particles aggregation, Brownian force was

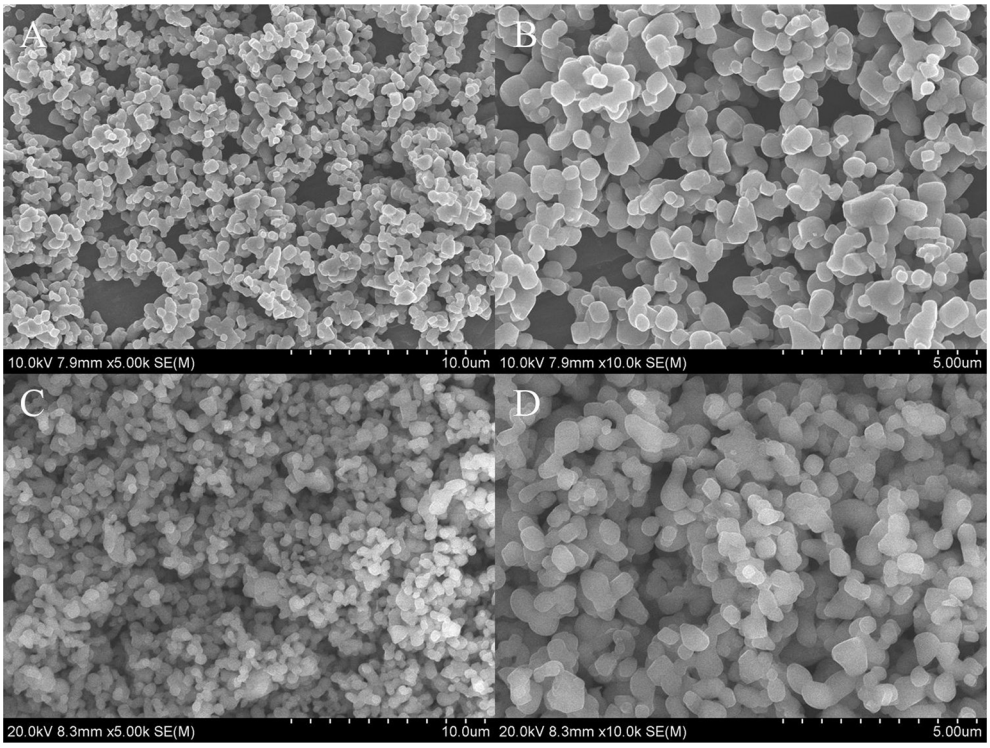

Fig. 4. SEM images of the obtained $Li_4Ti_5O_{12}$ powders without (A&B) and with (C&D) the pretreatment of USN process.

not enough to prevent sedimentation. Under these conditions, we successfully obtained smaller particle size of the $Li_4Ti_5O_{12}$ electrode with a smooth surface which may introduce more active sites for the charge transfer processes and further reduce the diffusion resistance of Li-ion and electron, thus the following promotion of the battery's electrochemical performance could be expected.

3.2. Electrochemical characterization

It is well known that the performance of $Li_4Ti_5O_{12}$ anode is closely related to the grain size, particle morphologies and crystallographic structure. To clarify the influence of the pretreatment process of USN on the electrochemical performance of the $Li_4Ti_5O_{12}$ prepared by a solid-state reaction process at calcination temperature of 800 °C for 7 h, multiple electrochemical tests were carried. To investigate the rate capability, the $Li_4Ti_5O_{12}$ anode with the activated process has been tested at various rates from 1C to 40C, and the results are presented in Fig. 6. The discharge/charge cycles were taken for 10 cycles at each rate. The first discharge capacities reached 181, 178, 163, 137, 107 and 76 mAh g^{-1} for the discharge rate is 1C, 2C, 5C, 10C, 20C and 40C, respectively. The capacities gradually drop with the increasing of discharge/charge rate, compared with other $Li_4Ti_5O_{12}$ electrode materials prepared by solid-state reaction in literature [4,31–34], as shown in Table 1, this $Li_4Ti_5O_{12}$ material possess much better high-rate performance. This result suggests that the high surface area and dispersion of $Li_4Ti_5O_{12}$ electrode material can increase the Li-ion extraction/insertion and electronic diffusion rate at high discharge/charge rate. Fig. 6 also shows the plateau voltage difference between charge and discharge is 20, 30, 40, 70, 110, 190 mV at the rate of 1C,

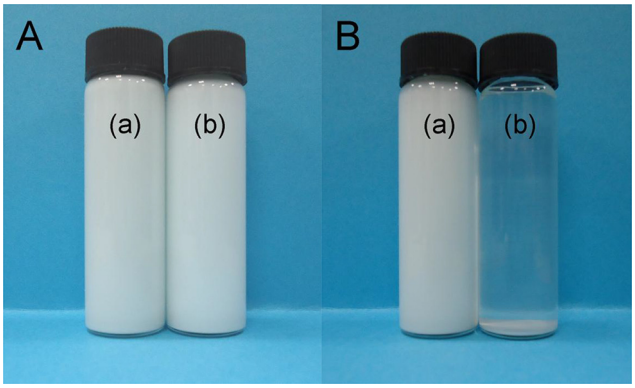

Fig. 5. The state of suspension (A) at the beginning and (B) after standing for five days.

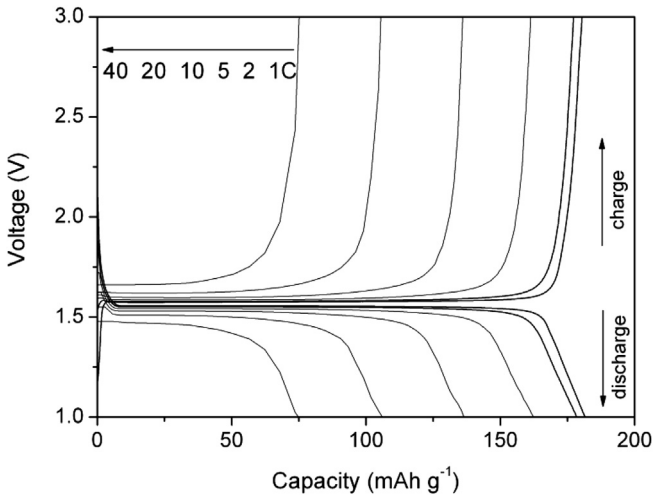

Fig. 6. Variation of the discharge capacities of the 800 °C for 7 h calcined $Li_4Ti_5O_{12}$ with the cycle voltage from 1 to 3 V at different discharge rates between 1C and 40C.

Table 1
The first discharge capacities of $Li_4Ti_5O_{12}$ materials prepared by solid-state reaction at the discharge/charge rate range between 1C and 40C ("–"means no data in related references).

	The first discharge capacity (mAh g^{-1}) at different rates					
	1C	2C	5C	10C	20C	40C
This study	**181**	**178**	**163**	**137**	**107**	**76**
Ref.4	155	144	95	70	55	37.5
Ref.31	164	157	146	130	–	–
Ref.32	170	160	139	112	81	52
Ref.33	152	144	123	110	93	76
Ref.34	150	146	106	88	–	–

2C, 5C, 10, 20C, 40C, respectively. It indicates that the polarization increases with the increasing of discharge/charge rate.

Fig. 7 shows the cyclical behaviour of the $Li_4Ti_5O_{12}$ sample before and after the pretreatment of USN process at various rates from 1C to 40C for 10 times. Stable capacities are observed even at a high-rate of 20C, it suggests the promising application of the USN pretreatment of nano and sub-micron powders are suitable for application in high-rate rechargeable Li-ion battery. Moreover, the rate capability has fluctuated slightly in the last few cycles at 40C discharge rate. This result may be attributed to the detachment of electrode powder from the current collector of the copper foil during the discharge/charge processes. Therefore, to further improve the stability of the cell, more work needs to be done. After 10 cycles, the capacity at 40C remains 42% of that at 1C for the pretreated $Li_4Ti_5O_{12}$ sample, but for the untreated one the capacity is only about 16%.

The long cycling behaviour of the cell with the $Li_4Ti_5O_{12}$ electrode at different discharge/charge rates of 0.5C, 1C and 2C was further carried out. For each stage, the process was taken with 100 cycles. As shown in Fig. 8, the stable discharged capacities were observed at each stage. After 100 discharge/charge cycles, the discharge capacity was 178, 179 and 175 at 0.5C, 1C and 2C, which was less than 0.008%, 0.007% and 0.01% discharge capacity loss of each cycle, respectively. It suggests good stability of the synthesized sub-micron $Li_4Ti_5O_{12}$ from the modified solid-state reaction method for rechargeable lithium battery. It's worth noting that the discharge capacity of $Li_4Ti_5O_{12}$ was slightly higher than the theoretical capacity at low rates, indicating possible lithium residing on surface/interface, cavities or other defects in the anode materials in addition to the regular intercalation/deintercalation.

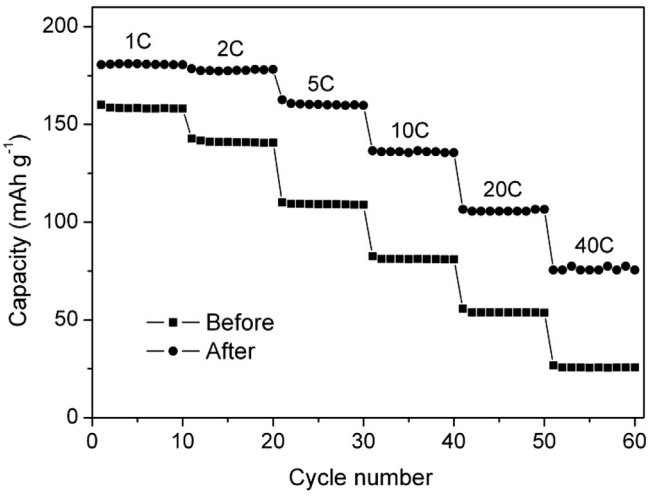

Fig. 7. The cyclical behaviour of the $Li_4Ti_5O_{12}$ samples before and after the pretreatment of USN process at various rates from 1C to 40C for 10 times.

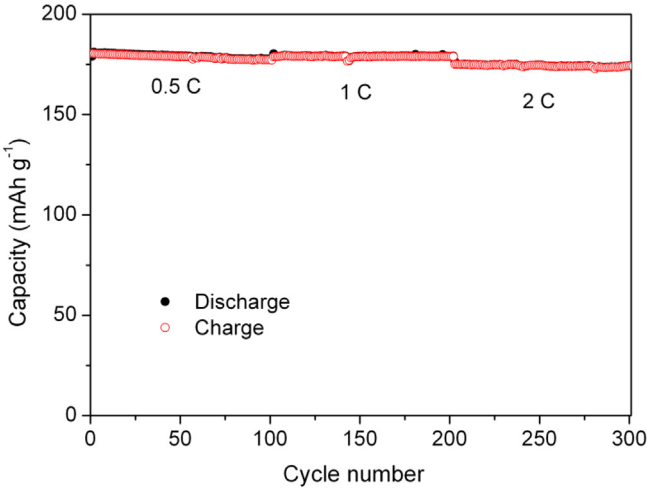

Fig. 8. The charge/discharge curves of the cells at 0.5C, 1C and 2C rate over the voltage range of 1.0–3.0 V for 100 cycles.

In order to recognize the essence of the electrode process kinetic behaviour clearly, electrochemical impedance spectroscopy (EIS) measurements were carried out at the initial voltage at room temperature. Fig. 9 shows the Nyquist plots of the $Li_4Ti_5O_{12}$ electrode before and after the pretreatment in the frequency range of 100 kHz to 0.1 Hz. Both Nyquist plots are comprised of a depressed semicircle in high-frequency range and a straight line in the frequency range below 2 Hz. It is well known that the high-frequency semicircle is related to the ohmic resistance of the cell from Z′ axis interception. The high-to-medium frequency intercept is attributed to the contact resistance, polarization resistance, charge transfer resistance and corresponding capacitances. The oblique line at the lower frequency range indicates the Warburg impedance of long-range Li-ion diffusion through the $Li_4Ti_5O_{12}$ electrode [7,35]. From Fig. 10, we can obtain the value of the Warburg impedance coefficient (σ_w). According to the following two equations:

$$Z_{re} = R_s + R_{ct} + \sigma_w \cdot \omega^{-0.5} \quad (1)$$

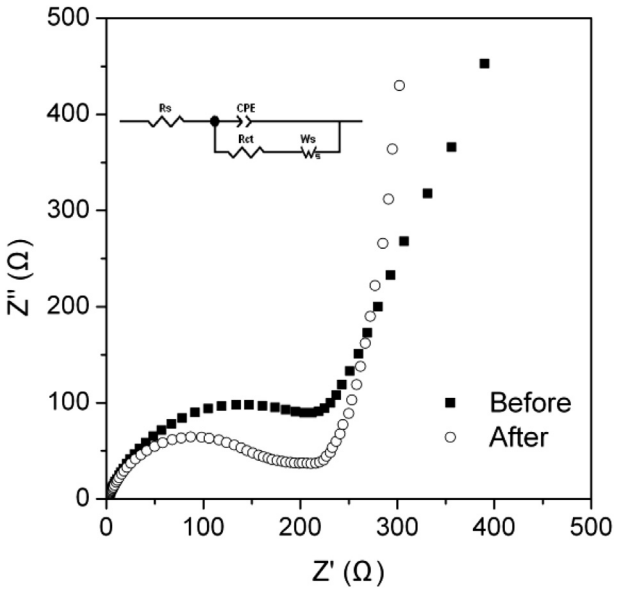

Fig. 9. Impedance spectra of the half-cell of the $Li_4Ti_5O_{12}$ electrode before and after the pretreatment in the frequency range of 100 kHz to 0.1 Hz.

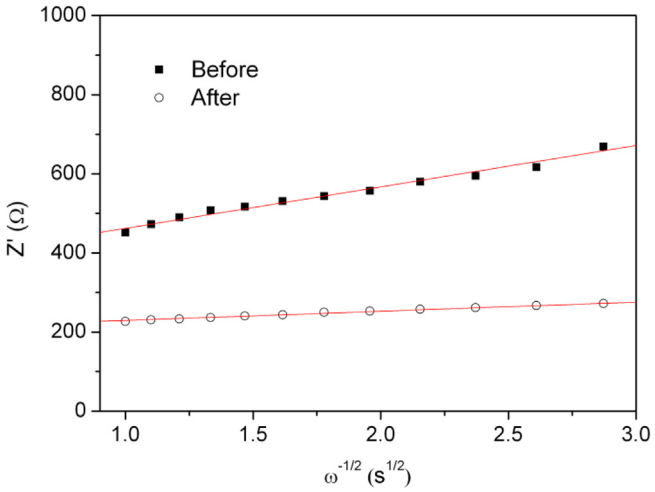

Fig. 10. Relationship between real impedance with the low frequencies for the $Li_4Ti_5O_{12}$ electrode before and after the pretreatment.

$$D = 0.5\left(\frac{RT}{AF^2\sigma_W C}\right)^2 \quad (2)$$

where R_s is attributed to the ohmic resistance of the electrolyte; R_{ct} indicates the charge transfer resistance at the active material interface; ω is angular frequency in the low frequency region; D is the Li-ion diffusion coefficient; R is the gas constant; T is the absolute temperature; F is the Faraday's constant; A is the area of the electrode surface; C is the molar concentration of Li-ions, the D can be calculated.

From Table 2, it can be seen that the R_{ct} for the pretreated $Li_4Ti_5O_{12}$ electrode (sample A, $R_s = 2.25\ \Omega$, $R_{ct} = 185\ \Omega$) is much smaller than the untreated one (sample B, $R_s = 2.34\ \Omega$, $R_{ct} = 249\ \Omega$). This result indicates that the charge transfer at the electrolyte/electrode interface is greatly improved after the pretreatment, and the overall cell internal resistance is also decreased. Based on Eq. (2), the larger σ_w, the slower Li-ion diffusion coefficient in the bulk electrode. As shown in Table 1, sample A has much higher ion conductivity than sample B. This should be ascribed to the fact that sample A has a larger surface area and less particle agglomerations than sample B. During our experiment, the values of R_{ct} and D are both lower than the untreated electrode material, which is in agreement with the excellent electrochemical performance of sub-micron crystalline $Li_4Ti_5O_{12}$. Thus, the USN process is a promising way to synthesise the high-rate anode material which have significantly improved electrochemical performance in lithium-ion battery.

4. Conclusions

Sub-micron $Li_4Ti_5O_{12}$ material has been successfully synthesized by a modified solid-state reaction method with the assistance of a USN process. The products, calcined at 800 °C for 7 h with the mole ratio of Li/Ti was 4.04:5, showed pure phase and good crystallinity with an average particle size of ~350 nm. This synthesis approach was relatively simple and effective to obtain the high dispersion and surface area material in the sub-micron range. The electrochemical performance of this $Li_4Ti_5O_{12}$ anode material exhibited excellent discharge capacity of 178 and 76 mAh g^{-1} at 2C and 40C discharge rate, respectively, and the discharge capacity at 40C remained 42% of that at 1C rate after 10 cycles. The EIS results demonstrate that the electrode performance has been improved due to the increasing ion conductivity. Besides, the excellent rate capability and cycling performance of $Li_4Ti_5O_{12}$ are mainly attributed to the micro morphology optimization. It indicates that the electrochemical performance of $Li_4Ti_5O_{12}$ exhibits a tendency to increase with increasing the electrode conductivity.

Table 2
EIS simulation parameters of $Li_4Ti_5O_{12}$ samples before and after the pretreatment of the USN process of the equivalent circuit correspond to the initial voltage of the cells.

Sample	R_s (Ω)	R_{ct} (Ω)	σ (Ω cm^2 s$^{-0.5}$)	D (cm^2 s^{-1})
A (After)	2.25	185	23.2	6.65E-13
B (Before)	2.34	249	104.7	3.26E-14

Acknowledgements

This work was supported by the National Natural Science Foundation of China under contract No. 21171116, the International Science & Technology Cooperation Program of China under contract No. 2012DFG11660 and the Shanghai Rising-Star Program (B-type) No. 14QB1402900.

References

[1] T. Ohzuku, A. Ueda, N. Yamamota, J. Electrochem. Soc. 142 (1995) 1431–1435.
[2] K. Zaghib, M. Simoneau, M. Armand, M. Gauthier, J. Power Sources 81-82 (1999) 300–305.
[3] E.M. Sorensen, S.J. Barry, H.K. Jung, J.R. Rondinelli, J.T. Vaughey, K.R. Poeppelmeier, Chem. Mater. 18 (2006) 482–489.
[4] T. Yuan, R. Cai, K. Wang, R. Ran, S. Liu, Z. Shao, Ceram. Int. 35 (2009) 1757–1768.
[5] A. Sivashanmugam, S. Gopukumar, R. Thirunakaran, C. Nithya, S. Prema, Mater. Res. Bull. 46 (2011) 492–500.
[6] H. Pan, L. Zhao, Y.S. Hu, H. Li, L. Chen, ChemSusChem 5 (2012) 526–529.
[7] Y.H. Rho, K. Kanamura, J. Solid State Chem. 177 (2004) 2094–2100.
[8] C.Y. Ouyang, Z.Y. Zhong, M.S. Lei, Electrochem. Commun. 9 (2007) 1107–1112.
[9] M. Kalbác, M. Zukalová, L. Kavan, J. Solid State Chem. 8 (2003) 2–6.
[10] W.J.H. Borghols, M. Wagemaker, U. Lafont, E.M. Kelder, F.M. Mulder, J. Am. Chem. Soc. 131 (2009) 17786–17792.
[11] N. Zhang, Z. Liu, T. Yang, C. Liao, Z. Wang, K. Sun, Electrochem. Commun. 13 (2011) 654–656.
[12] L. Shen, X. Zhang, E. Uchaker, C. Yuan, G. Cao, Adv. Energy Mater. 2 (2012) 691–698.
[13] L. Cheng, J. Yan, G.N. Zhu, J.Y. Luo, C.X. Wang, Y.Y. Xia, J. Mater. Chem. 20 (2010) 595–602.
[14] G.J. Wang, J. Gao, L.J. Fu, N.H. Zhao, Y.P. Wu, T. Takamura, J. Power Sources 174 (2007) 1109–1112.
[15] Z. Liu, N. Zhang, Z. Wang, K. Sun, J. Power Sources 205 (2012) 479–482.
[16] M. Krajewski, M. Michalska, B. Hamankiewicz, D. Ziolkowska, K.P. Korona, J.B. Jasinski, M. Kaminska, L. Lipinska, A. Czerwinski, J. Power Sources 245 (2014) 764–771.
[17] S. Huang, Z. Wen, Z. Gu, X. Zhu, Electrochim. Acta 50 (2005) 4057–4062.
[18] K. Kanamura, N. Akutagawa, K. Dokko, J. Power Sources 146 (2005) 86–89.
[19] P. Kubiak, A. Garcia, M. Womes, L. Aldon, J.O. Fourcade, P.E. Lippens, J.C. Jumas, J. Power Sources 119–121 (2003) 626–630.
[20] A.D. Robertson, H. Tukamoto, J.T.S. Irvine, J. Electrochem. Soc. 146 (1999) 3958–3962.
[21] Y. Qi, Y. Huang, D. Jia, S. Bao, Z.P. Guo, Electrochim. Acta 54 (2009) 4772–4776.
[22] S. Huang, Z. Wen, X. Zhu, Z. Gu, Electrochem. Commun. 6 (2004) 1093–1097.
[23] M. Ganesan, M.V.T. Dhananjeyan, K.B. Sarangapani, N.G. Renganathan, J. Electroceram 18 (2007) 329–337.
[24] Z. Lin, X. Hu, Y. Huai, L. Liu, Z. Deng, J. Suo, Solid State Ionics 181 (2010) 412–415.
[25] T.F. Yi, L.J. Jiang, J. Liu, M.F. Ye, H.B. Fang, A.N. Zhou, J. Shu, Ionics 17 (2011) 799–803.
[26] C.Y. Lin, Y.R. Jhan, J.G. Duh, J. Alloy. Compd. 509 (2011) 6965–6968.
[27] E. Matsui, Y. Abe, M. Senna, A. Guerfi, K. Zaghib, J. Am. Ceram. Soc. 91 (2008) 1522–1527.
[28] A. Guerfi, S. Sévigny, M. Lagacé, P. Hovington, K. Kinoshita, K. Zaghib, J. Power Sources 119-121 (2003) 88–94.
[29] G. Wang, J. Xu, M. Wen, R. Cai, R. Ran, Z. Shao, Solid State Ionics 179 (2008) 946–950.
[30] N. He, B. Wang, J. Huang, J. Solid State Chem. 14 (2010) 1241–1246.
[31] X. Li, H. Hu, S. Huang, G. Yu, L. Gao, H. Liu, Y. Yu, Electrochim. Acta 112 (2013) 356–363.
[32] D. Wang, C. Zhang, Y. Zhang, J. Wang, D. He, Ceram. Int. 39 (2013) 5145–5149.
[33] T. Yuan, R. Cai, Z. Shao, J. Phys. Chem. C. 115 (2011) 4943–4952.
[34] C. Lin, J. Duh, J. Alloy. Compd. 509 (2011) 3682–3685.
[35] C. Ho, I.D. Raistrick, R.A. Huggins, J. Electrochem. Soc. 127 (1980) 343–350.